Journal of Physics B: Atomic,
Molecular and Optical Physics

Ionization of helium by 64.6 eV electrons

J. Phys. B: At. Mol. Opt. Phys. **43** (2010) 074028 (8pp) doi:10.1088/0953-4075/43/7/074028

Ionization of helium by 64.6 eV electrons

I Bray, T Lepage, D V Fursa and A T Stelbovics

ARC Centre for Antimatter-Matter Studies, Institute of Theretical Physics, Curtin University of Technology, GPO Box U1987 Perth, Western Australia 6845, Australia

Received 11 September 2009, in final form 2 November 2009
Published 19 March 2010
Online at stacks.iop.org/JPhysB/43/074028

Abstract
A comprehensive computational study using the convergent close-coupling method of 64.6 eV electron-impact ionization of the ground state of helium is presented. The kinematics considered range from the very asymmetric energy-sharing through to equal energy-sharing. The cross sections given range from the total to fully differential, with the latter being calculated for in- and out-of-plane geometries. Generally excellent agreement with available experiment is found, but some systematic discrepancies are also identified.

(Some figures in this article are in colour only in the electronic version)

1. Introduction

The electron–helium scattering problem is one of the most fundamental collision systems in atomic physics. Owing to the ease with which the target beam can be prepared there is an abundance of experimental data for excitation and ionization processes, for vastly varying kinematical conditions and geometrical orientation of the detectors. In recent years, there has been immense development in complete theories of electron–atom collisions, but mostly for the electron-atomic hydrogen problem. The exterior complex scaling (ECS) method [1–4], the time-dependent close-coupling (TDCC) [5] are able to yield accurate *e*–H excitation and ionization cross sections at all energies of interest. However, as yet the ECS method has not yet been extended to *e*–He collisions, whereas the TDCC method does so within the configuration average approach [6] making the distinction between the singlet- and triplet-state excitation not possible. We do note, however, the successful application of the TDCC approach to *e*–He ionization; see [7] and references therein. As far as we are aware only the convergent-close-coupling (CCC) method is able to treat both the *e*–H [8, 9] and *e*–He [10, 11] systems for all of the excitation and (single) ionization processes, with the validity of the method being independent of the kinematical conditions.

Historically, the close-coupling method was intended for just excitation processes, and various *R*-matrix implementations dominate the literature; see for example [12–15]. The CCC method was also initially intended just for excitation processes, but following the description of the *e*–H total ionization cross section [16], the method has been extended to fully differential ionization [17]. This work was initially modelled [18] on the pioneering effort of Curran and Walters [19], but then considerably simplified to yield the ionization amplitudes directly from the excitation amplitudes of the positive-energy pseudostates [17].

Application of the CCC method to ionization has resulted in some greater understanding of the close-coupling expansion utilizing a complete basis. The ionization amplitudes were found to converge to step functions [20], and for finite bases they behave as Fourier expansions of step functions [21]. This required a slight modification of the way the amplitudes are used to define the cross sections, particularly for the equal-energy sharing case, where the amplitudes converge to half the step height [21, 22]. Furthermore, the numerical success of the CCC and ECS methods has resulted in a comprehensive analysis of the underlying formal issued involving Coulomb two- and three-body problems [23].

The CCC method has been applied extensively to *e*–He (single) ionization at the higher energies [17] through to the more difficult lower energies [22]. The case of 64.6 eV electron-impact ionization of helium is of particular value to the field owing to the extraordinary amount of absolute data for varying kinematics and geometries. We demonstrate here how a single CCC calculation is able to generate results for comparison with all of the available data. The comprehensive study will uncover some unexpected discrepancies with experiment not previously identified.

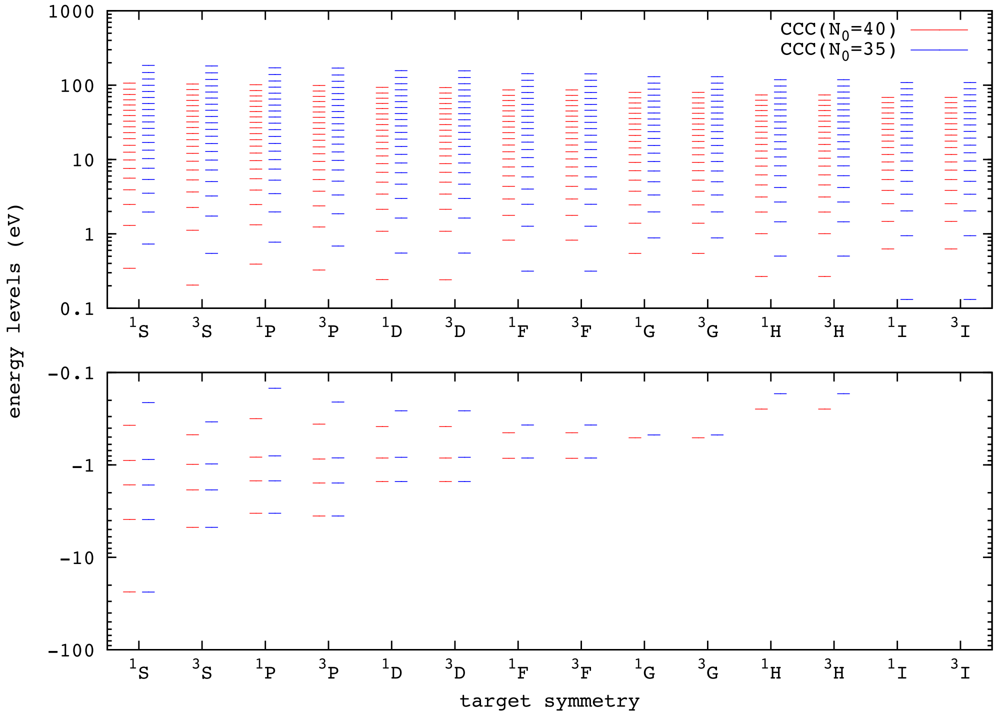

Figure 1. Energy levels, relative to the ground state energy of He^+, obtained in the two CCC calculations; see the text for details.

2. Convergent close-coupling theory for *e*–He scattering

The details of electron–helium scattering calculations with the CCC method were presented by Fursa and Bray [10]. We begin with an overview of the target structure generation.

2.1. Target structure

The helium wavefunctions are written in the frozen-core approximation where one of the electrons is described by the $He^+(1s)$ orbital. The other electron is represented as a linear combination of N_l orthogonal Laguerre basis functions, obtained by diagonalizing the He^+ Hamiltonian for each orbital angular momentum $l \leqslant l_{\max}$. The two-electron states are obtained upon diagonalization of the He Hamiltonian, using a subset of the Laguerre-based orbitals, for each l and spin s. To make convergence studies rather systematic, we take the Laguerre basis size to be $N_0 - l$, and so convergence needs to be established just with increasing $l_{\max}$ and N_0. Note that we keep the Laguerre exponential parameter $\lambda = 4$ constant so that the $He^+(1s)$ orbital comes out exactly. The resulting states are all square-integrable and have both negative- and positive-energy states. With increasing N_0 the former converge to the true discrete states and the latter yield an increasingly dense discretization of the target continuum. Due to the frozen-core approximation, the ground state ionization energy is 23.8 eV rather than the experimental energy of 24.6 eV. However, all of the excited states are very accurately treated by the frozen-core approximation, and a small shift in the incident energy ensures that in the calculations and the experiment the total energy E is the same. Figure 1 presents the energy levels ε_n of the helium wavefunctions used in the present CCC calculations with $l_{\max} = 6$ and $N_0 = 35$ and 40. We have not used all of the $N_0 - l$ orbitals in the generation of the He states, but only $25 - l$. Given that the incident energy is 64.6 eV there is no point keeping the very high energy orbitals that will lead to high-energy He states. The two N_0 calculations have exactly the same number of states (309), but the lower value of N_0 leads to a slightly less dense discretization and hence extends out to higher energies.

2.2. Scattering calculation

The two-electron target states are used to expand the total wavefunction of the *e*–He system, and thereby uniquely define the close-coupling approximation for the scattering calculation. There are several numerical methods for solving such systems. In the CCC method we solve a set of partial-wave expanded coupled Lippmann–Schwinger equations in momentum space [8]. The present combination of 309 states and $l_{\max} = 6$ leads to a maximum of 1179 coupled channels, and when combined with integration over intermediate momentum, results in having to solve linear equations with 80 000 by 80 000 matrices.

Solution of the equations results in scattering amplitudes $T_{fi}(\boldsymbol{k}_f, \boldsymbol{k}_i)$ for the transition from the initial He state of energy ε_i to the final He state of energy ε_f due to an electron of incident momentum $\boldsymbol{k}_i$ and outgoing momentum $\boldsymbol{k}_f$. For $\varepsilon_f < 0$ this can be used directly to generate discrete excitation data for comparison with experiment. However, for ionization ($\varepsilon_f > 0$) we multiply $T_{fi}(\boldsymbol{k}_f, \boldsymbol{k}_i)$ by the overlap of the Laguerre-based two-electron state with the corresponding true continuum (frozen-core) state [17]. Then the resulting ionization amplitude may be written as $T(\boldsymbol{k}_A, \boldsymbol{k}_B, \boldsymbol{k}_i)$, where $\boldsymbol{k}_A = \boldsymbol{k}_f$ and $\boldsymbol{k}_B$ is defined from $E_B = \varepsilon_f$ for each l [17].

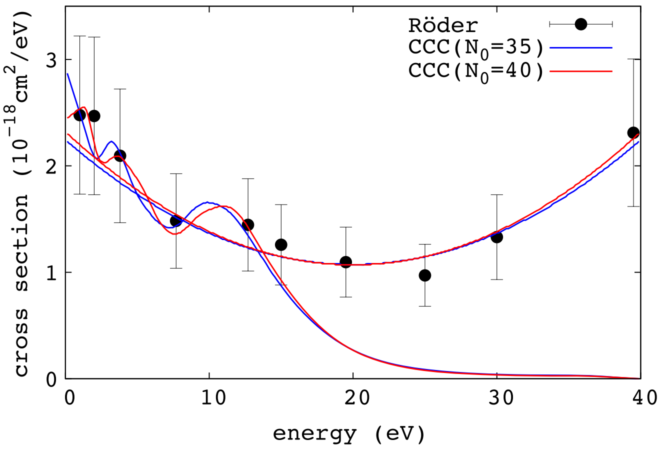

Figure 2. Singly differential cross sections for 64.6 eV electron-impact single-ionization of helium. The raw CCC results are those that show oscillation at the lower energies and diminish to zero at the higher energies. The symmetric, about 20 eV, results are the corresponding estimates of the true cross section; see the text. The experimental data are due to Röder *et al* [26].

3. Results

3.1. Total ionization cross section (TICS)

We begin with the CCC results for the TICS. This can be obtained simply by summing the cross sections for excitation of all of the positive-energy states. We obtained $2.97 \times 10^{-17}\text{cm}^2$ with the $N_0 = 40$ calculation and $2.90 \times 10^{-17}\text{cm}^2$ with the $N_0 = 35$ one. These values are within the (few per cent) error bars of Montague *et al* [24] and Shah *et al* [25].

3.2. Singly differential cross section (SDCS)

In figure 2, we present the CCC results for the SDCS. For both calculations, there are two curves, corresponding to the raw results (which go to zero above 20 eV) and the estimates (which are symmetric about 20 eV) of the SDCS. The CCC theory is unitary and yields independent cross sections for $0 \leqslant \varepsilon_f \leqslant E$, where presently $E = 40$ eV. The integral under the raw CCC curves yields the TICS given above. Knowing [20–22] that the CCC results should converge to the true SDCS, but only on the interval $0 \leqslant \varepsilon_f < E/2$, together with the value of the SDCS at $E/2$ (raw amplitude converges to half step height, hence cross section to a quarter) allows us to make the symmetrized estimates. The symmetrized results also smooth the oscillations as these arise from a Fourier-like expansion of the underlying step function. Subsequently, the generation of the angle-differential cross sections for asymmetric energy-sharing kinematics needs to be rescaled by the ratio of the estimated and raw results. This is typically by less than 10%, but ensures internal consistency of the cross sections and that the convergence checks are not overly influenced by the expected oscillations. For example, the two SDCS estimates are in good agreement with each other even though the nature of the oscillations is a little different at the lower energies.

3.3. Doubly differential cross section (DDCS)

In figure 3 the DDCS are presented. The measured DDCS were integrated over the solid angle to generate the SDCS

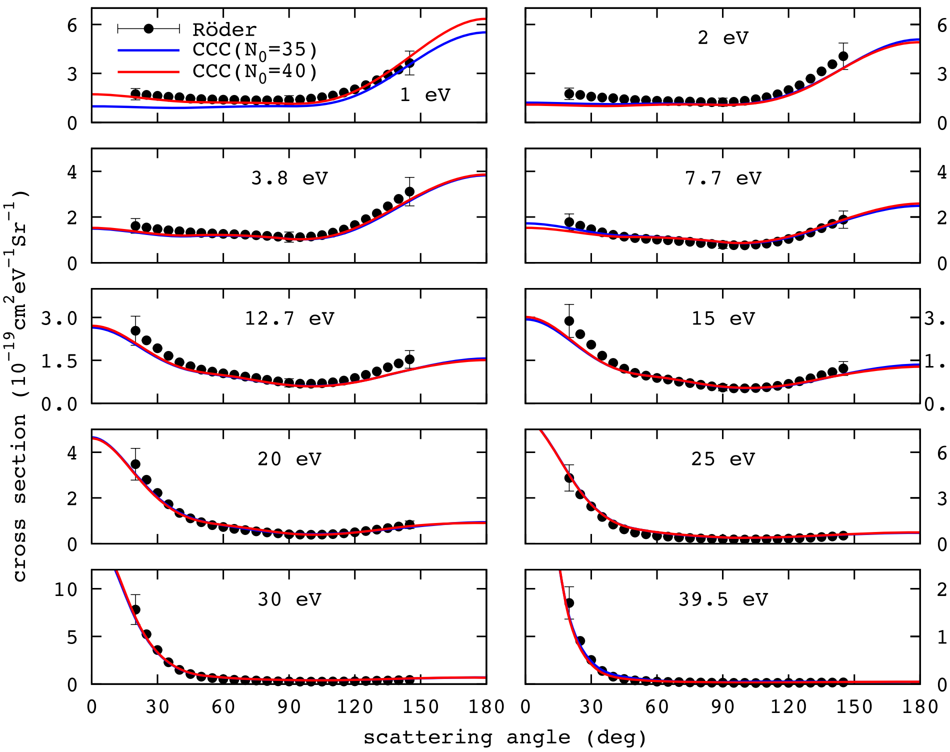

Figure 3. Doubly differential cross sections for 64.6 eV electron-impact ionization of helium. The CCC calculations are described in the text. The experimental data are due to Röder *et al* [26].

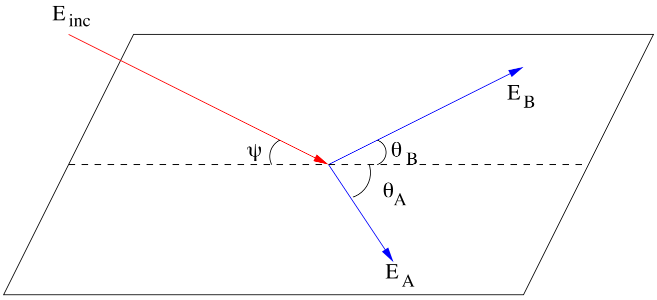

Figure 4. Parametrization of the fully differentialionization cross sections.

of figure 2. We see an excellent agreement between the two calculations and the experiment. The only minor exception to this is at the lowest energy of 1 eV, where there is some visible difference between the two calculations. This is due to the fact that the smaller N_0 calculation has a less dense discretization making the generation of the ionization amplitudes more problematic.

3.4. Triply differential cross section (TDCS)

The TDCS are obtained by measuring the two outgoing electrons in coincidence. They have been obtained for a range of kinematics and varying geometric orientation of the detectors; see figure 4. For the case of equal-energy sharing, i.e. two 20 eV outgoing electrons, we have a detailed study of the in-plane geometries by Röder with 25% absolute value uncertainty [27], and out-of-plane geometries by Murray and Read with 44% absolute value uncertainty [28]. The data for both sets of measurements are internormalized, and one geometry is common to both sets. To enable comparison with theory we have multiplied the data of Röder by 1.2, as was done in [22], and multiplied the data of Murray and Read by 0.77 to ensure agreement at the common angle of 90°. This is a convenient angle for normalization as the statistical uncertainty is very small, and is the unique point common to all of the considered out-of-plane geometries.

Figures 5 and 6 show the TDCS in the case of coplanar geometry and equal-energy sharing. In the former, the angle θ_A of one outgoing electron is fixed and the TDCS is plotted against the angle θ_B of the other electron. For the latter, the angle $\theta_{AB} = \theta_B - \theta_A$ between the two outgoing electrons is kept constant and the TDCS is plotted against the scattering angle θ_B. We see an excellent agreement between the two calculations and the experiment.

In figure 7, the out-of-plane (for $\psi > 0°$) geometries are considered. Here the two detectors are on the opposite side of the incident beam which comes in at angle ψ to the scattering plane; see figure 4. The geometry is such that the $\theta_B = -\theta_A = 90°$ point is common for all ψ. The in-plane case for $\psi = 0°$ has also been measured by Röder. Note that uniformly multiplying the data of Röder by 1.2 for best visual fit on the previous two figures and then normalizing the data of Murray and Read at 90° to the theory means that we are not free to move the two data sets for $\psi = 0°$ relative to each other. While the 90° point is near a minimum for $\psi = 0°$ it is the maximum for $\psi = 90°$. Hence we are identifying a systematic discrepancy between the CCC theory and the data of Murray and Read. Most unusually, the discrepancy is for the largest cross sections measured. Whereas for $\psi = 90°$

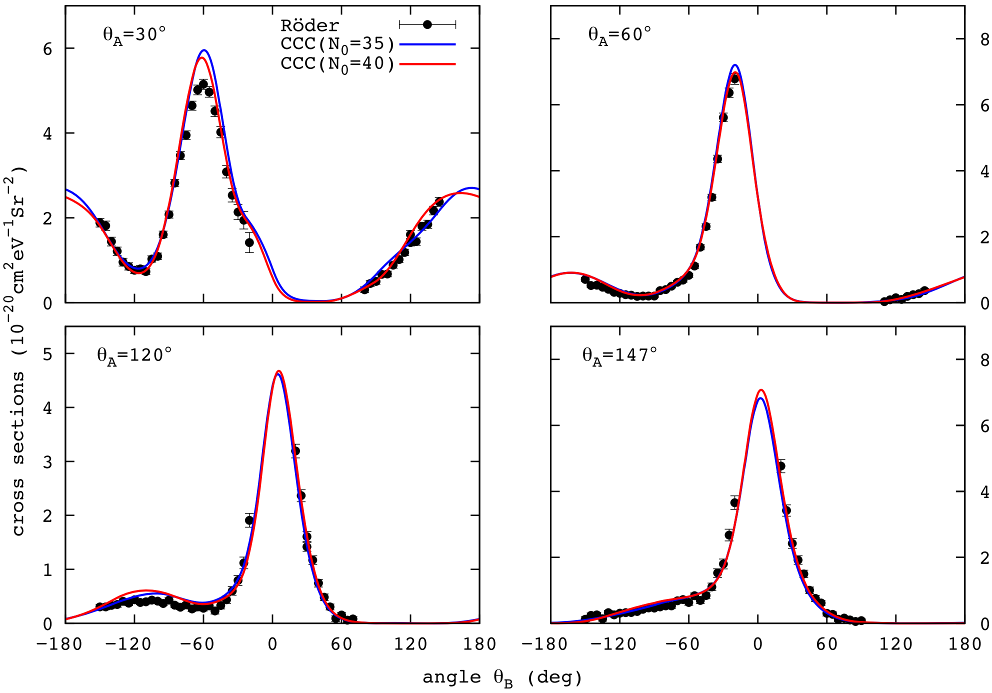

Figure 5. Triply differential cross sections at fixed angle θ_A for 64.6 eV electron-impact ionization of helium with two 20 eV outgoing electrons. The experimental data due to Röder, see [27], have 25% absolute uncertainty and have been multiplied by 1.2 for best visual fit to the theory.

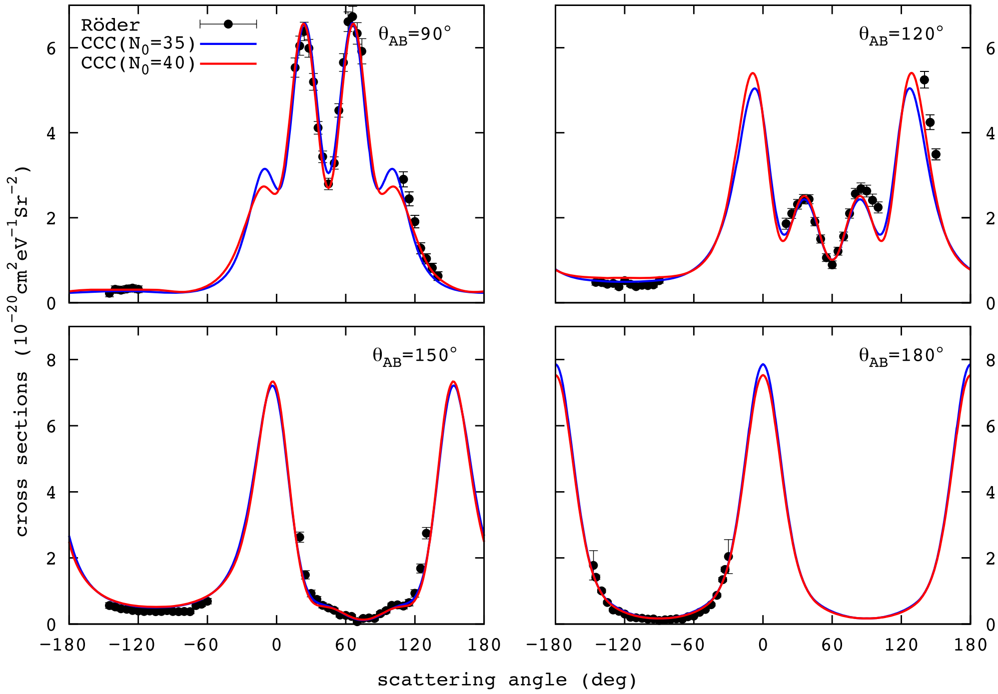

Figure 6. As for figure 5, except for fixed θ_{AB}.

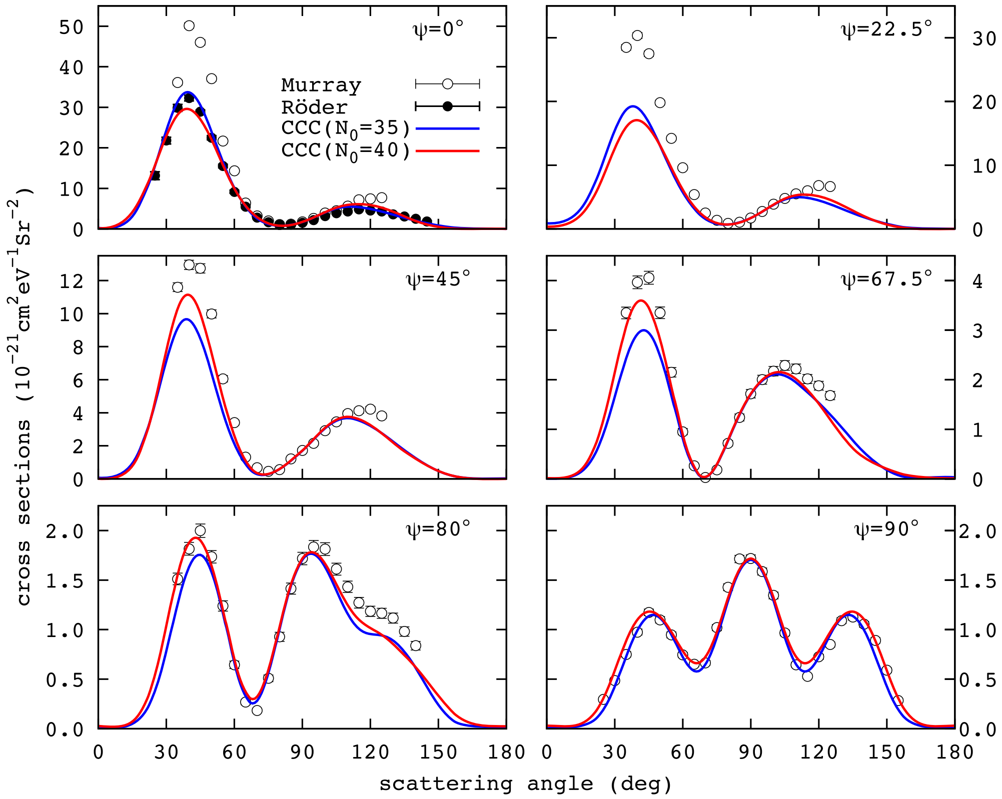

Figure 7. As for figure 5 except for the geometries measured by Murray and Read [28], whose data have been normalized to the theory at the common 90° angle; see the text.

agreement with experiment is within 0.1 of the presented units, the discrepancy for $\psi = 0^\circ$ is around 20 units. We shall see that a similar systematic problem persists for asymmetric energy sharing.

In figure 8, the outgoing electrons do not share the excess energy equally, having $E_A = 25$ eV and $E_B = 15$ eV, though the geometry remains the same as for figure 7. This time only the data of Murray and Read [28] are available. Again

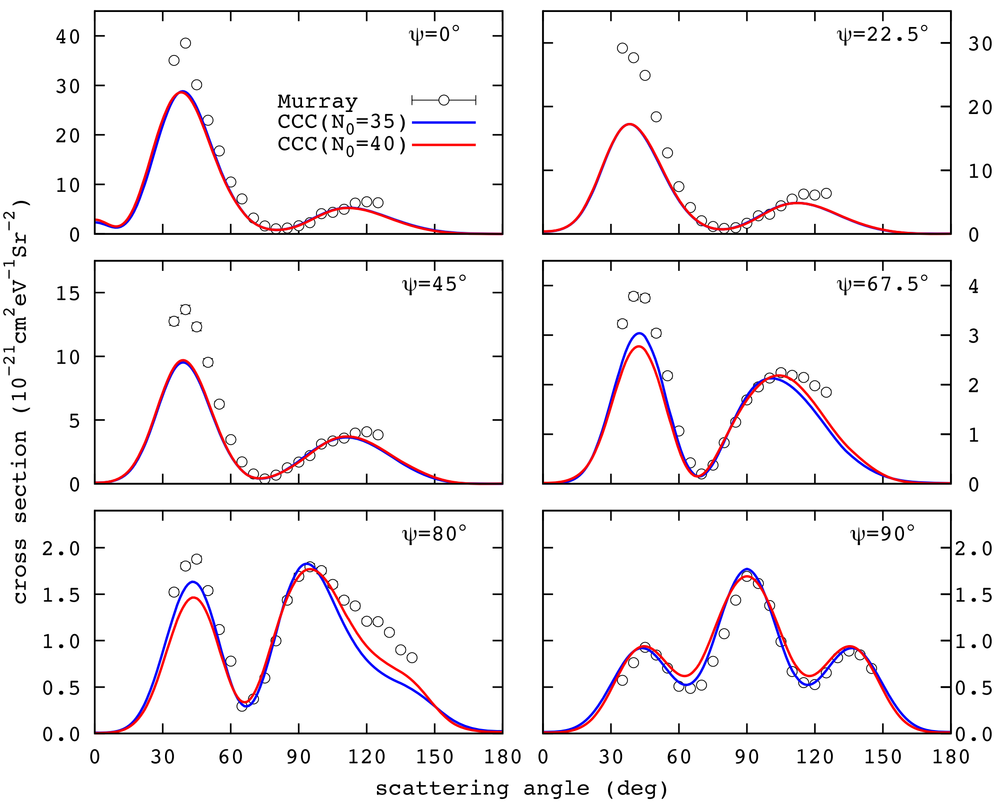

Figure 8. Triply differential cross sections for 64.6 eV electron-impact ionization of helium with $E_A = 25$ eV and $E_B = 15$ eV outgoing electrons. The experimental data of Murray and Read [28] have an uncertainty of about 44% and have been multiplied by 0.59 to be normalized to the theory at the common (for all ψ) 90° angle.

we normalize the experiment to the theory at the common point of 90°, by multiplication of the original data by 0.59. Convergence of the two calculations is excellent, particularly for the largest cross sections (smallest ψ). However, as for the equal-energy sharing case, agreement with experiment is best for the smallest cross sections.

Figure 9 presents the results for $E_A = 30$ eV and $E_B = 10$ eV kinematics. Once again we find good convergence between the two calculations, and best agreement with the smallest measured cross sections. This time the discrepancy with the largest cross sections has increased to around 30 of the presented units.

Finally, figure 10 shows the comparison for the case of $E_A = 35$ eV and $E_B = 5$ eV kinematics. Much the same observation can be made as for the previous three figures. However, it is interesting to note the qualitative change in the $\psi = 0°$ cross section at the forward angles. Owing to electron–electron repulsion this region should have small cross sections whenever the electrons have similar energies. Even for the previous case of $E_A = 30$ and $E_B = 10$ eV the cross sections here were small. Yet the transition to $E_A = 35$ and $E_B = 5$ eV has resulted in this region to be a clear maximum. It is most unfortunate that we have a systematic discrepancy with experiment here and such a rapid variation predicted by theory is not able to be confirmed.

There are other interesting behaviour in the TDCS that we have not yet touched upon. This involves the deep minima of the cross sections at intermediate scattering angles for certain values of ψ. This arises from the destructive interference of the various partial waves and has been studied in some detail recently by Colgan *et al* [29] at a range of incident energies.

4. Summary and conclusions

We presented the results of two 64.6 eV e–He CCC calculations, concentrating only on the ionization processes. Excellent agreement with the TICS, SDCS and DDCS has been demonstrated. Excellent agreement has also been found with the coplanar TDCS measured by Röder, which are available only for equal energy-sharing kinematics. While we find excellent agreement with the data of Murray and Read for the smallest most out-of-plane kinematics, there are substantial discrepancies for the largest most in-plane cross sections. This is true for equal and asymmetric energy-sharing kinematics.

We are unable to suggest any reason for the identified discrepancies. While it is not unusual to find discrepancies with experiment for the smallest cross sections, this is the first time we have come across agreement with the smallest cross sections measured and not the largest. We do not expect the frozen-core treatment of the ground state in the CCC calculations to be responsible for the discrepancy. Generally, the smaller the cross section, the more accurate the calculation needs to be. Here we see that the smallest out-of-plane cross sections are very well described by the present calculations. This, together with the agreement of the CCC results and the experimental TICS, SDCS, DDCS and the in-plane data

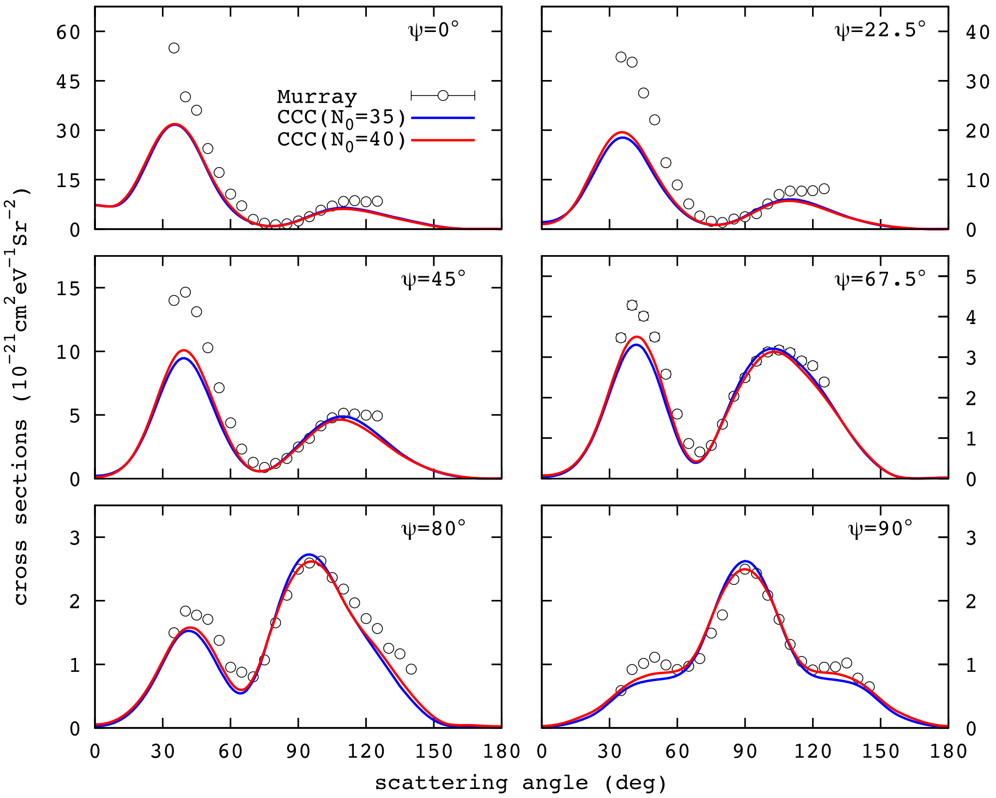

Figure 9. Same as for figure 8, except for $E_A = 30$ eV and $E_B = 10$ eV. The normalization constant is 0.72.

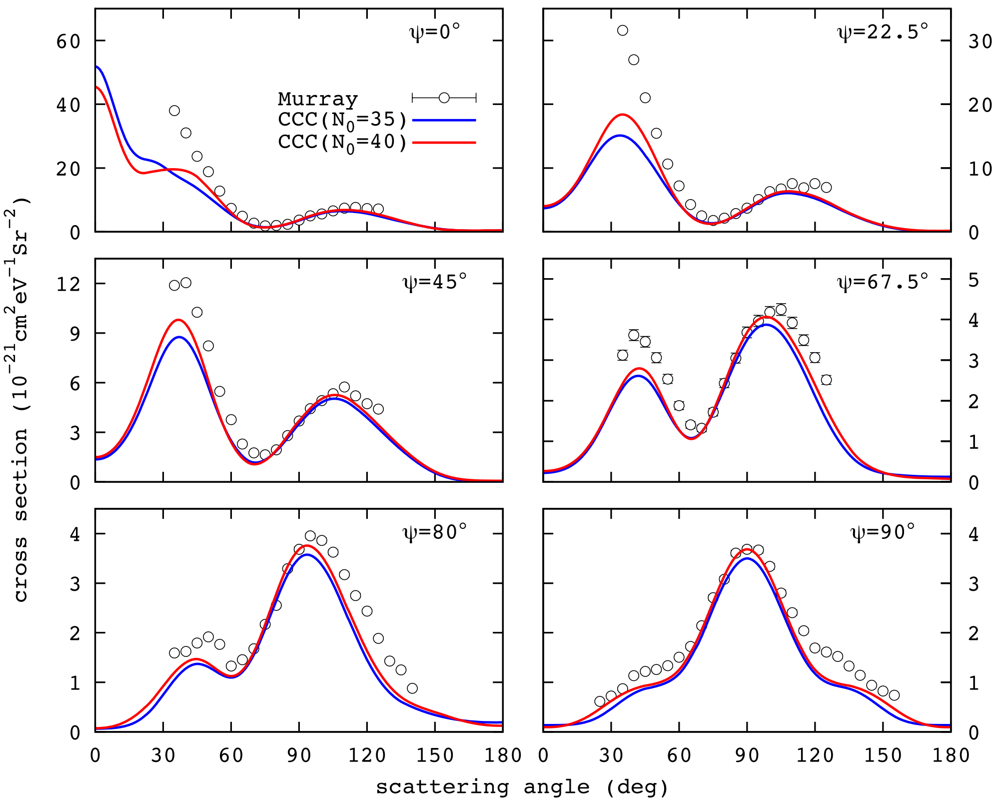

Figure 10. Same as for figure 8, except for $E_A = 35$ eV and $E_B = 5$ eV. The normalization constant is 0.84.

of Roeder, suggests that the frozen-core approximation is sufficiently accurate. We are hopeful that the discrepancies, presented here in full detail for the first time, will stimulate experimental activity aimed at their resolution.

Acknowledgments

This work was supported by the Australian Research Council. We are grateful for access to the Australian National Computing Infrastructure Facility and its Western Australian node iVEC.

References

[1] Rescigno T N, Baertschy M, Isaacs W A and McCurdy C W 1999 *Science* **286** 2474–9
[2] Baertschy M, Rescigno T N and McCurdy C W 2001 *Phys. Rev.* A **64** 022709
[3] Bartlett P L, Stelbovics A T and Bray I 2004 *J. Phys. B: At. Mol. Opt. Phys.* **37** L69
[4] Bartlett P L 2006 *J. Phys. B: At. Mol. Opt. Phys.* **39** R379–R424
[5] Colgan J and Pindzola M S 2006 *Phys. Rev.* A **74** 012713
[6] Pindzola M S *et al* 2007 *J. Phys. B: At. Mol. Opt. Phys.* **40** R39–R60
[7] Colgan J, Foster M, Pindzola M S, Bray I, Stelbovics A T and Fursa D V 2009 *J. Phys. B: At. Mol. Opt. Phys.* **42** 145002
[8] Bray I and Stelbovics A T 1992 *Phys. Rev.* A **46** 6995–7011
[9] Bray I and Stelbovics A T 1995 *Adv. At. Mol. Phys.* **35** 209–54
[10] Fursa D V and Bray I 1995 *Phys. Rev.* A **52** 1279–98
[11] Fursa D V and Bray I 1997 *J. Phys. B: At. Mol. Opt. Phys.* **30** 757–85
[12] Burke P G and Robb W D 1975 *Adv. At. Mol. Phys.* **11** 143–214
[13] Fon W C, Berrington K A, Burke P G and Kingston A E 1981 *J. Phys. B: At. Mol. Phys.* **14** 1041–51
[14] Bartschat K, Hudson E T, Scott M P, Burke P G and Burke V M 1996 *J. Phys. B: At. Mol. Opt. Phys.* **29** 115–23
[15] Gorczyca T W and Badnell N R 1997 *J. Phys. B: At. Mol. Opt. Phys.* **30** 3897–912
[16] Bray I and Stelbovics A T 1993 *Phys. Rev. Lett.* **70** 746–9
[17] Bray I and Fursa D V 1996 *Phys. Rev.* A **54** 2991–3004
[18] Bray I, Konovalov D A, McCarthy I E and Stelbovics A T 1994 *Phys. Rev.* A **50** R2818–R2821
[19] Curran E P and Walters H R J 1987 *J. Phys. B: At. Mol. Phys.* **20** 337–65
[20] Bray I 1997 *Phys. Rev. Lett.* **78** 4721–4
[21] Stelbovics A T 1999 *Phys. Rev. Lett.* **83** 1570–3
[22] Stelbovics A T, Bray I, Fursa D V and Bartschat K 2005 *Phys. Rev.* A **71** 052716
[23] Kadyrov A S, Bray I, Mukhamedzhanov A M and Stelbovics A T 2009 *Ann. Phys.* **324** 1516–46
[24] Montague R G, Harrison M F A and Smith A C H 1984 *J. Phys. B: At. Mol. Phys.* **17** 3295–310
[25] Shah M B, Elliot D S, McCallion P and Gilbody H B 1988 *J. Phys. B: At. Mol. Opt. Phys.* **21** 2751–61
[26] Röder J, Ehrhardt H, Bray I and Fursa D V 1997 *J. Phys. B: At. Mol. Opt. Phys.* **30** 1309–22
[27] Bray I, Fursa D V, Röder J and Ehrhardt H 1997 *J. Phys. B: At. Mol. Opt. Phys.* **30** L101–L108
[28] Murray A J and Read F H 1993 *J. Phys. B: At. Mol. Opt. Phys.* **26** L359–L365
[29] Colgan J, Al Hagan O, Madison D H, Murray A J and Pindzola M S 2009 *J. Phys. B: At. Mol. Opt. Phys.* **42** 171001